Raw clays from Morocco for degradation of pollutants by Fenton-type reaction for water treatment

O. Assila[1,2], Z. Bencheqroun[1,3], E. Rombi[4], T. Valente[5], A.S. Braga[5], H. Zaitan[3], A. Kherbeche[2], O.S.G.P. Soares[6,7], M.F.R. Pereira[6,7], A.M. Fonseca[1,8], P. Parpot[1,8], I.C. Neves[1,8,*]

[1]CQUM, Centre of Chemistry, Chemistry Department, University of Minho, Campus de Gualtar, 4710-057, Braga, Portugal

[2]Laboratory of Catalysis, Process, Materials and Environment, School of Technology, University Sidi Mohammed Ben Abdellah Fez, Morocco

[3]Processes, Materials, Environment Laboratory (LPME), Department of Chemistry, Faculty of Sciences and Technology, Sidi Mohamed Ben Abdellah University, Fez, BP. 2202, Morocco

[4]Dipartimento di Scienze Chimiche e Geologiche, University of Cagliari, Complesso Universitario di Monserrato, 09042 Monserrato, Italy

[5]ICT, Institute of Earth Sciences, Pole of the University of Minho, 4710-057 Braga, Portugal

[6]LSRE-LCM - Laboratory of Separation and Reaction Engineering – Laboratory of Catalysis and Materials, Faculty of Engineering, University of Porto, Portugal

[7]ALiCE - Associate Laboratory in Chemical Engineering, Faculty of Engineering, University of Porto, Portugal

[8]CEB - Centre of Biological Engineering, University of Minho, Campus de Gualtar, 4710-057 Braga, Portugal

Abstract

Three raw clays from Morocco were used as heterogeneous catalysts for Fenton-type oxidation of organic pollutants in water. The selected pollutants were two dyes used in the textile industry, Congo Red (CR) and Tartrazine (Tar, known also as a food coloring compound, E102) and Caffeine (Caf), a stimulant drug present in popular beverages such as coffee and tea, commonly used in Morocco. Two different processes were used for their degradation: (i) Fenton-type reaction; and (ii) electro-Fenton-type reaction. Process (i) was used for Tar and Caf degradation in the presence of clays from different region of Morocco (Middle Atlas - $Clay_{MA}$, Fez - $Clay_{F}$, and Ourika - $Clay_{O}$), the best results being obtained with $Clay_{O}$ and $Clay_{MA}$, on which 60.0 and 23.4 % of conversion and 41.0 and 20.5 % of mineralization were achieved for Tar and Caf, respectively. Process (ii) was used for degrading CR by clay-modified electrodes (CME) using the rawclays from Fez and Ourika regions ($Clay_{F}$ and $Clay_{O}$). The stability of the CME was assessed by cyclic voltammetry studies, which proved that they are stable in the experimental conditions used. The electrodegradation of CR dye, performed without hydrogen peroxide in the reaction medium, achieve 67.0 % of mineralization at the end of electrolysis (2 h).

1. Introduction

The 2030 Agenda for Sustainable Development with its 17 sustainable development goals (SDGs) from the United Nations (UN) aims to end poverty, conserve biodiversity, combat climate change and improve the livelihoods of people everywhere (Axon and James, 2018; United Nations, 2016). In the 17 SDGs, water and the use of raw materials are interlinked, and chemistry and geochemistry are two of the keys to achieve these goals in order to preserve society and the planet for the future generations (Anastas and

Zimmerman, 2016; United Nations, 2023). Moroccan raw clays were utilized as heterogeneous catalysts to eliminate pollutants from effluents in order to tackle the issue of clean water through the valorization of raw materials via the oxidation Fenton reaction. Morocco is a country with important deposits of clays and these geological materials are very attractive to apply as adsorbents (Bencheqroun et al., 2019a) or heterogeneous catalysts for Fenton-type oxidation (Assila et al., 2023).

Porous materials as clays offer a word of possibilities for preparing heterogeneous catalysts due to their stability in different pH ranges, easily separation, and reutilization. Clays are a group of minerals used as raw materials in the ceramic, paper, and metal industries, in the field of pet feeding, and as adsorbents, discoloration agents, ion exchangers, supports, and catalysts. These minerals are phyllosilicates with basic building blocks of $Si(O, OH)_4$ tetrahedra and $M(O, OH)_6$ octahedra, and mostly M = Al^{3+}, Mg^{2+} or $Fe^{2+,3+}$ (Assila et al., 2023; Bencheqroun et al., 2019a; Schoonheydt, 1991).

Fenton-type oxidation reaction is very attractive, non-toxic nature, ease to use, and low cost (Fida et al., 2017; Fu et al., 2022; Liu et al., 2021, Wang and Tang, 2021). However, there are few examples using clays as modified electrodes for degradation of pollutants by electro Fenton-type oxidation. Electrochemistry is one of the sustainable methods to be used for the treatment of waste effluents; indeed, it does not require high temperatures, allows the achievement of high degrees of mineralization of the pollutants, and has low operational costs (Brillas et al., 2009; Chaplin, 2014). A further advantage comes from the possibility of carrying out the electrochemical process using electrodes modified with heterogeneous catalysts, due to their peculiar properties (Poza-Nogueiras et al., 2018).

The works of Ozcan *et al*. (2017) showed that iron in the kaolin clay is capable to degrade the emerging pollutant enoxacin with a TOC of 98 % after 7 h of reaction. Methylene blue was also degraded with the clay modified electrode with a COD of 96.5% after 45 min of reaction (Ma et al., 2009). Modified electrodes using iron oxide supported on nanostructured allophane clays, with both Fe^{3+} and Fe^{2+} species on the surface, were used for degrading atrazine with higher efficiency compared to the heterogeneous Fenton-type catalysis (Garrido-Ramírez et al., 2013). The clay modified electrodes (CME) combine the advantages of the catalytic properties of the clay structures with the versatility, energy efficiency, cost effectiveness, and facility for process automation of the electrochemical processes (Herney-Ramirez et al., 2010).

Herein we report the degradation of different pollutants by Fenton-type reaction and electro Fenton-type oxidation using several raw clay minerals from Morocco. The places where the clays come from cover an important part of Morocco territory (Fig. 1), which confirms the presence of huge deposits of clay minerals in this country.

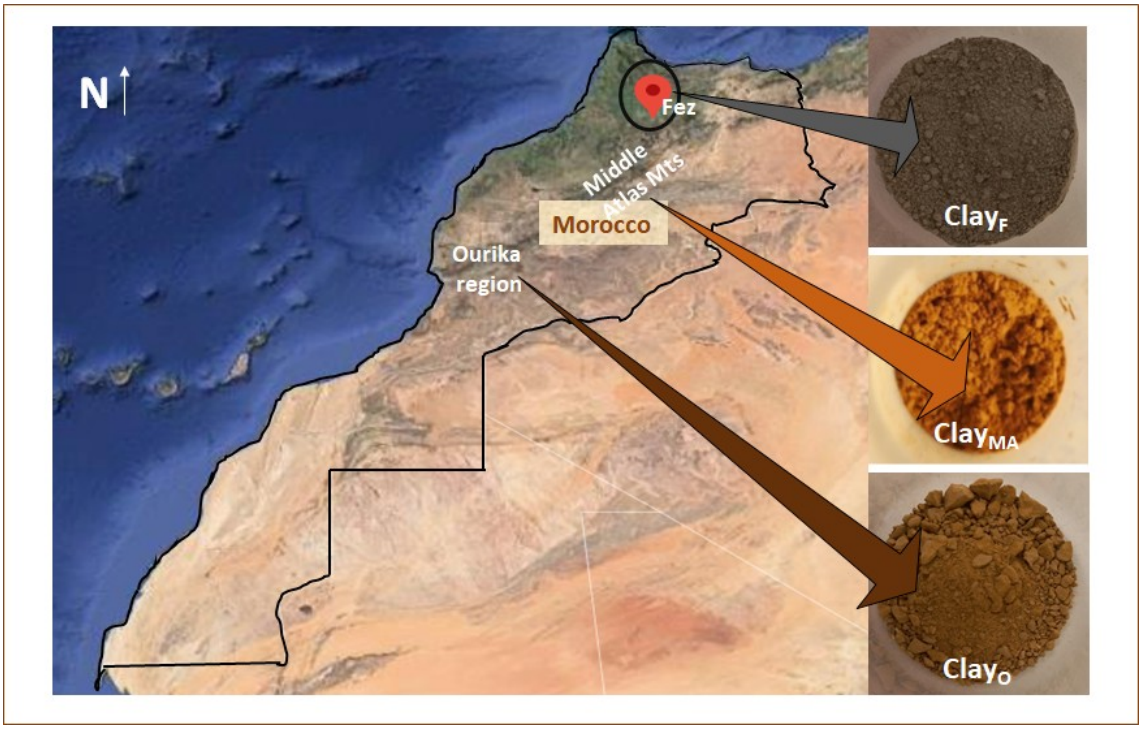

Fig. 1. Map of Morocco showing the location of the clays sites.

Two clays were collected from the Ourika region ($Clay_O$) and the city of Fez city ($Clay_F$), while one sample was collected from the Middle Atlas region ($Clay_{MA}$) and were used for studied the degradation of pollutants in water. Tartrazine (Tar) and caffeine (Caf) were removed by Fenton-type reaction using the three raw clays and Congo Red (CR) was degraded by electro Fenton-type oxidation of using CME based on $Clay_O$ and $Clay_F$.

2. Experimental section

2.1. Preparation and characterization of the heterogeneous clay catalysts

Three raw clays from Morocco obtained from deposits located in the Middle Atlas region ($Clay_{MA}$, where MA stands for Middle Atlas), the city of Fez ($Clay_F$, where F stands for Fez), and the Ourika region ($Clay_O$, where O stands for Ourika) were used in this study without any prior activation. Samples were ground, sieved to obtain particle sizes (60 - 100 μm), and washed with distilled water. After that, all clays were dried at 60 ºC for 24 h and stored in hermetic plastic bottles until further use.

The heterogeneous clay catalysts were prepared by addition of zinc or copper using an adapted method described in (Assila et al., 2023). In order to study the effect of the presence of the metal in the clay, aqueous solutions (250 mL) containing the same metal amounts ($2.70x10^{-2}$ mmol of Cu or Zn) were mixed with 4 g of the pristine support ($Clay_{MA}$) at pH 4.0. The suspensions were stirred during 24 h at room temperature. After each ion-exchange step, the suspensions were filtered-off, washed with deionized water and dried at 60 ºC overnight. Finally, the solids were calcined at 350 °C during 4 h under a dry-air stream. The samples were identified Cu-$Clay_{MA}$ and Zn-$Clay_{MA}$. All clay samples were used as heterogeneous catalysts for the degradation of tartrazine (Tar,

$C_{16}H_9N_4Na_3O_9S_2$ ≥ 90%, Sigma-Aldrich) and caffeine (Caf, $C_8H_{10}N_4O_2$ ≥ 99%, Sigma-Aldrich) in Fenton-type reaction. In addition, $Clay_F$ and $Clay_O$ were used for preparing clay modified electrodes (CME) for the degradation of Congo Red (CR, $C_{32}H_{22}N_6Na_2O_6S_2$, 3,3′-([1,1′-biphenyl]-4,4′-diyl)bis(4-aminonaphthalene-1-sulfonic acid, Sigma-Aldrich) by electro Fenton-type oxidation.

The heterogeneous clays catalysts based in raw clays from Morocco were characterized by different techniques, such as powder X-ray diffraction (XRD), X-ray photoelectron spectroscopy (XPS), Fourier transform infrared spectroscopy (FTIR), N_2 adsorption, scanning electron microscopy coupled with energy dispersive X-ray analysis (SEM/EDX), and chemical analysis.

Mineralogical identification were performed by XRD through a Philips X'pert Pro-MPD diffractometer (Philips PW 1710, APD), provided with automatic divergence slit and graphite monochromator, using CuKα radiation powdered at 40 kV and 40 mA ($Cuk_{\alpha 1}$ = 1.54060 Å and $Cuk_{\alpha 2}$ = 1.54443 Å). The XRD patterns were obtained from powders (bulk sample) and from oriented aggregates (< 2 μm), in the range of 2θ from 3 to 65 and 3 to 35°, respectively with step size of 0.02° and counting time of 1.25 s. Sample preparation for XRD analysis involved gentle grinding of solid into a fine powder and packing of approximately 1.0 g of the sample into the sample holder. Identification of clay minerals was obtained in the oriented aggregates after chemical and thermal treatments (ethylene glycol saturation and heating at 490 °C).

XPS analysis was performed by recording the high and survey spectra with a Kratos Axis-Supra instrument. Monochromatic X-ray source Al Kα (1486.6 eV) was used for all samples and experiments. The residual vacuum in the X-ray analysis chamber was maintained at around $7.2x10^{-9}$ torr. The samples were fixed to the sample holder with double sided carbon tape. Due to the non-conducting nature of the samples, it was

139 necessary to use a co-axial electron neutralizer to minimize surface charging, which
140 performed the neutralization by itself. Charge referencing was done by setting the
141 binding energy of C1s photo peak at 285.0 eV C 1s hydrocarbon peak. Photoelectrons
142 were collected from a take-off angle of 90º relative to the sample surface. The
143 measurement was done in a Constant Analyser Energy mode (CAE) with a 10 mA of
144 emission current and 160 eV pass energy for survey spectra and 20 eV pass energy for
145 high resolution spectra. A wide scan survey spectrum was used to identify and quantify
146 the elements in the sample. High-resolution narrow scans are used to build the chemical
147 state assessment, as well as to quantify the presence of the reference elements in each
148 sample. Data analysis and atomic quantification were determined from the XPS peak
149 areas using the ESCApe software supplied by the manufacturer Kratos Analytical.
150 Nitrogen (N_2) adsorption-desorption isotherms were measured at -196 °C on
151 ASAP2040 Micrometrics device endowed with a thermal conductivity detector. The
152 prepared samples were previously degassed at 90 °C for 1 h and then at 250 °C with a
153 heating rate of 5 °C min-1 for 6 h, up to a residual pressure smaller than 0.5 Pa. The
154 specific surface area and pore size distribution (PSD) were determined by the Brunauer-
155 Emmett-Teller (BET) method and Barret-Joyner-Halenda (BJH) analysis, respectively,
156 using the adsorption branch.
157 SEM/EDX analysis was performed on a Phenom ProX with EDS detector (Phenom-
158 World BV, Netherlands). All data were acquired using the ProSuite software integrated
159 with Phenom Element Identification software, allowing the quantification of the
160 concentration of the elements present in the samples, expressed in either weight or
161 atomic percentages. The samples were added to aluminum pin stubs with electrically
162 conductive carbon adhesive tape (PELCO Tabs™) and were imaged without coating.
163 The aluminum pin stub was then placed inside a Phenom Charge Reduction Sample

Holder (CHR), and different points were analyzed for elemental composition. EDS analysis was conducted at 15 kV with intensity map.

Chemical analysis was performed by inductively coupled plasma optical emission spectroscopy (ICP-OES) for the quantification of metals in the liquid phase during the ion-exchange process using a Optima 8000 spectrometer (PerkinElmer). A 5110 ICP-OES spectrometer (Agilent Technologies) was instead used to quantify the metals in the solid samples.

2.2 Fenton-type oxidation

For the degradation of Tar or Caf with the different heterogeneous clay catalysts, the concentration of pollutant (30 ppm), temperature (40 ºC), and pH (=3.0) were fixed at the best values found in a preliminary study in a stirred semi-batch reactor at atmospheric pressure using $Clay_{MA}$ as catalyst (Assila et al., 2023). Prior to experiments, all catalysts were pretreated at 100 °C for 2 h in an oven. The semi-batch reactor was loaded with 250 mL of a solution of pollutant prepared with ultrapure water produced with an ultrapure water system (Milli-Q, EQ 7000), using 200 mg of catalyst and 5 mL of H_2O_2 (12 mM). The reaction was then performed under stirring at 300 rpm, during 300 min. Sampling was carried out at fixed time intervals and the reaction was stopped with the addition of an excess of sodium sulphite (Na_2SO_3, Sigma-Aldrich), which instantaneously consumes the unreacted H_2O_2. Catalytic tests were performed in duplicate, and the maximum deviation observed in the removal of the organic pollutants was 2%.

2.3 Electro Fenton-type oxidation

Clays modified electrodes (CME) were prepared using $Clay_F$ and $Clay_O$ by the procedure already described in previous papers (Assila et al., 2023; Ferreira et al., 2018). Typically, CME were prepared by dispersing 20 mg of the clays powders in a mixture of 180 µL ultrapure water (Barnsted E-pure system, 18.2 MΩ cm at 20 °C) and 180 µL Nafion® suspension (5 wt. %, Sigma-Aldrich). The resulting suspensions were homogenized using an ultrasound bath and totally deposited onto the wet proofed Carbon Toray paper (CT, geometrical area of 4.0 cm^2, Quintech); the solvent was then evaporated at room temperature overnight. CT paper was glued to the platinum wire using a conductive carbon cement (Quintech) and subsequently dried at room temperature during 24 h.

A thermostat three-electrode cell assembly composed of a Hg/Hg_2Cl_2 (sat. KCl) reference electrode, a platinum foil (99.95%) counter electrode, and a CME working electrode were used for electrochemical measurements. The reference electrode consisted of a Saturated Calomel Electrode (SCE) Hg/Hg_2Cl_2 (sat. KCl) separated from the solution by a Habber-Luggin capillary tip. The electrochemical instrumentation consisted of a potentiostat/galvanostat from Amel Instruments coupled to a microcomputer (Pentium II/ 500 MHz) through an AD/DA converter. The Labview software (National Instruments) and a PCI-MIO-16E-4 I/O module were used for generating and applying the potential program as well as for acquiring data, such as current intensities.

Prior to electrochemical measurements, the solution is de-aerated with ultra-pure N_2 (U Quality from Air Liquide) for 30 min, and a nitrogen stream is maintained over the solution during the measurements in order to avoid any dissolved oxygen interferences. The electrocatalytic activity of CME was investigated by using cyclic voltammetry (CV) both in the absence and in the presence of the CR dye. In the CVs, the currents

were normalized with the geometrical surface area of the working electrode to provide more useful correlations in terms of kinetic issues. Electrolysis at a constant potential (2 V) in the presence of dye was carried out in the same electrolytic cell used for the CV studies. The used concentrations of the CR dye was $3.44x10^{-3}$ mmol (25 ppm) for the CV studies and $6.88x10^{-3}$ mmol (50 ppm) for electrolysis in 0.10 M NaCl solution, at room temperature without addition of hydrogen peroxide.

2.5 Product analysis

In order to quantify the extent of degradation of the organic pollutants by Fenton-type reaction, after separation of the solid catalyst by centrifugation, an UV-vis spectrophotometer (UV-2501PC from Shimadzu) was used at the characteristic wavelengths λ_{max} = 427 nm and 272 nm for Tar and Caf, respectively, in order to determine the residual concentration of the pollutant in the reaction solution.

Liquid phase samples from electro Fenton-type reaction were analyzed by high performance liquid chromatography (HPLC), equipped with an isocratic pump (Jasco PU-980 Inteligent HPLC Pump) and a double on-line detection including an UV-vis detector (Jasco Inteligent UV/vis detector). Separation of the different components was carried out using the following HPLC ion exchange columns: IonPac AS11-HC from Analytical, Aminex HPX-87 H (λ=210 and 260 nm) from Biorad, and RP18 from Merck (λ=497 nm).

The total organic carbon (TOC) was determined using the NPOC method, with a Shimadzu's Total Organic Carbon Analyzer TOC-L coupled with the ASI-L autosampler of the same brand.

3. Results and Discussion

3.1 Characterization of the heterogeneous clay catalysts

SEM investigated the morphology of the raw clays and the textural properties were evaluated by N_2 adsorption analysis (Fig. 2). SEM images show a heterogeneous morphology, with the presence of aggregates composed by particles of different size, with $Clay_{MA}$ having the smallest particles. All clays exhibit an isotherm type IIb, according to the IUPAC classification, with a hysteresis loop at high P/P_0 values, typical for mesoporosity originating from interparticles voids (Bergaya, 1995; Kloprogge, 2998; Weidler, 1997). Fig. 2 displays the N_2 isotherms and pore size distribution curves obtained for $Clay_F$ and $Clay_O$ as examples, while Table 1 shows the results obtained for all clays.

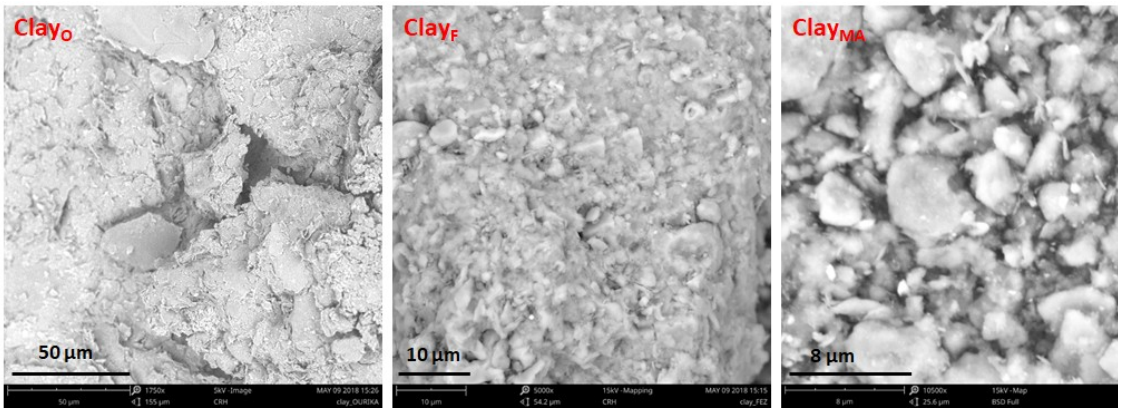

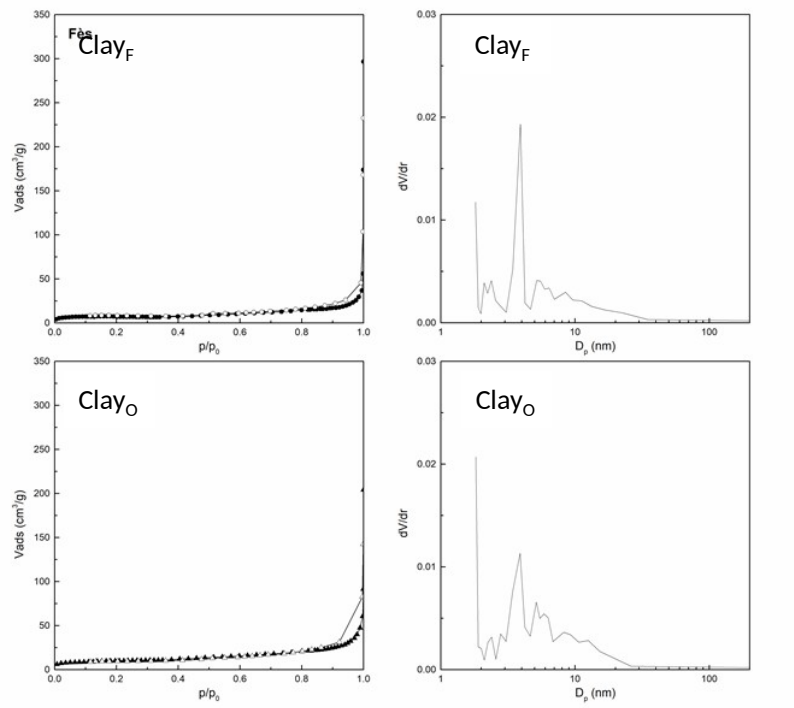

Fig. 2. SEM images of the pristine clays, N_2 adsorption/desorption isotherms and pore size distribution curves of $Clay_F$ and $Clay_O$.

The specific surface area obtained by the BET method is 22.5, 23.0 and 34.4 m^2/g for $Clay_F$, $Clay_{MA}$ and $Clay_O$, respectively and the latter being 1.5 times greater than the first. The largest volume has been determined for $Clay_O$, follow by $Clay_F$ and $Clay_{MA}$.

Table 1. Textural properties of the pristine clays.

Samples	S_{BET}[a] (m^2/g)	V_{total}[b] (cm^3/g)
$Clay_F$	22.5	0.060
$Clay_O$	34.4	0.090
$Clay_{MA}$	23.0	0.039

[a]Surface area calculated from the BET equation
[b]Total pore volume determined from the amount adsorbed at $P/P_o = 0.99$

The distribution of the pore diameters is obtained using the BJH method based on a discrete analysis of the adsorption branch of the isotherm, where the average pore diameters are 3.8 and smaller than 6 or 18.6 nm for $Clay_F$, $Clay_O$ and $Clay_{MA}$, respectively. These values confirm a mesoporous structure, typical of the materials formed between the elementary clay structures that are called tactoids (Bencheqroun et al., 2019a; Jiang et al., 2019).

$Clay_{MA}$ was modified by introduction of copper and zinc in order to enhance the catalytic behavior of the pristine clay. The composition of all clays was determined by ICP-OES analysis, with Si, Al and Fe as the most important elements. Ca, K, Ti and Mg, also typical elements of clay materials, were also quantified (Table 2).

Table 2. ICP-OES results (wt% of metals) of pristine clays and the two samples, Cu-$Clay_{MA}$ and Zn-$Clay_{MA}$.

Sample	Si (wt%)	Al (wt%)	Na (wt%)	K (wt%)	Mg (wt%)	Ca (wt%)	Fe (wt %)	Cu (wt%)	Zn (wt%)	Ti (wt%)
$Clay_{MA}$	27.06	12.05	0.25	3.68	1.86	3.69	5.40	-	-	0.51
Cu-$Clay_{MA}$	27.60	11.35	0.28	2.61	0.58	0.23	4.55	0.43	-	0.43
Zn-$Clay_{MA}$	27.39	11.31	0.31	2.87	0.63	0.33	4.33	-	0.32	0.46
$Clay_F$	23.88	5.93	0.62	1.47	1.72	11.44	3.98	-	0.35	0.29
$Clay_O$	26.43	9.89	0.31	2.52	0.96	0.35	6.45	-	-	0.50

$Clay_{MA}$ and $Clay_O$ contain higher amounts of Fe (5.40 and 6.45 wt.%, respectively), whereas $Clay_F$ is richer in calcium (11.44 wt.%). These differences in composition justifies the different colours of the clays (Fig. 1). The presence of iron in the pristine clays is expected to enhance the catalytic properties of these materials for Fenton-type

279 reactions. In the case of $Clay_{MA}$, the introduction of Cu or Zn leads to a remarkable
280 decrease in the Ca and Mg contents (about 90 and 70%, respectively); a more limited
281 variation is instead observed for K, Fe, and Ti, whose contents decrease by about 20, 30,
282 and 15%, respectively.
283 All these samples were analyzed by XPS to determine the composition, the relative
284 distribution, and the oxidation state of the components present on the surface. In
285 agreement with ICP-OES analysis, the predominant elements in all the recorded survey
286 XPS resolution spectra are oxygen (O 1s), carbon (C 1s), iron (Fe 2p), silicon (Si 2p),
287 and aluminum (Al 2s), typical for clay minerals (Elmi et al., 2016). In addition, small
288 amounts of potassium (K 2p), calcium (Ca 2p), and sodium (Na 1s) were also detected.
289 The binding energies (BE) of the principal elements as well as their surface amounts (wt
290 %) are reported in Table 3.
291
292 **Table 3.** Binding energies (BE) and the amount of the elements (wt%) obtained from
293 the XPS resolution spectra in the C 1s, O 1s, Cl 2p, N 1s and Ag 3d regions of
294 the samples.

Sample	$Clay_O$		$Clay_F$		$Clay_{MA}$	
peak	BE (eV)	wt (%)	BE (eV)	wt (%)	BE (eV)	wt (%)
Si 2p	102.56	24.71	102.96	27.24	102.73	23.75
Al 2s	119.26	9.24	119.46	7.42	119.53	10.04
O 1s	531.76	50.59	532.06	51.33	532.03	49.96
C 1s	285.06	5.30	285.06	6.77	285.13	6.60
Fe $2p_{1/2}$	724.36	1.96	725.76	1.72	725.83	1.37
Fe $2p_{3/2}$	711.76	1.99	712.66	1.33	711.93	1.76
Fe 3p	56.14	2.03	56.25	1.01	55.91	1.58

295

296 It can be noted that the BE values are similar for all the elements irrespective of the
297 pristine clay. By converse, some differences exist between the clays in the surface
298 concentration of the different components, which are linked to the geological deposits
299 where these materials came from. In particular, the surface amount of iron is in the
300 order $Clay_O$ (5.98 wt%) > $Clay_{MA}$ (4.71 wt%) > $Clay_F$ (4.06 %). The comparison with
301 the chemical analysis results (Table 2) shows similar Fe contents both on the surface
302 and in the bulk, indicating that it is homogeneously distributed throughout the clays
303 particles.
304 The energy separations (ΔE) between both peaks of Fe 2p is 12.6, 13.1 and 13.9 eV, for
305 $Clay_O$, $Clay_F$ and $Clay_{MA,}$ respectively, and the presence of the Fe 3p peak suggests the
306 existence of iron in different oxidation states. For all clay samples, the high XPS spectra
307 of iron show that both peaks measured in the survey spectra in the region of Fe $2p_{1/2}$ and
308 Fe $2p_{3/2}$ can be deconvoluted in three and four components for each, respectively (Fig.
309 3).

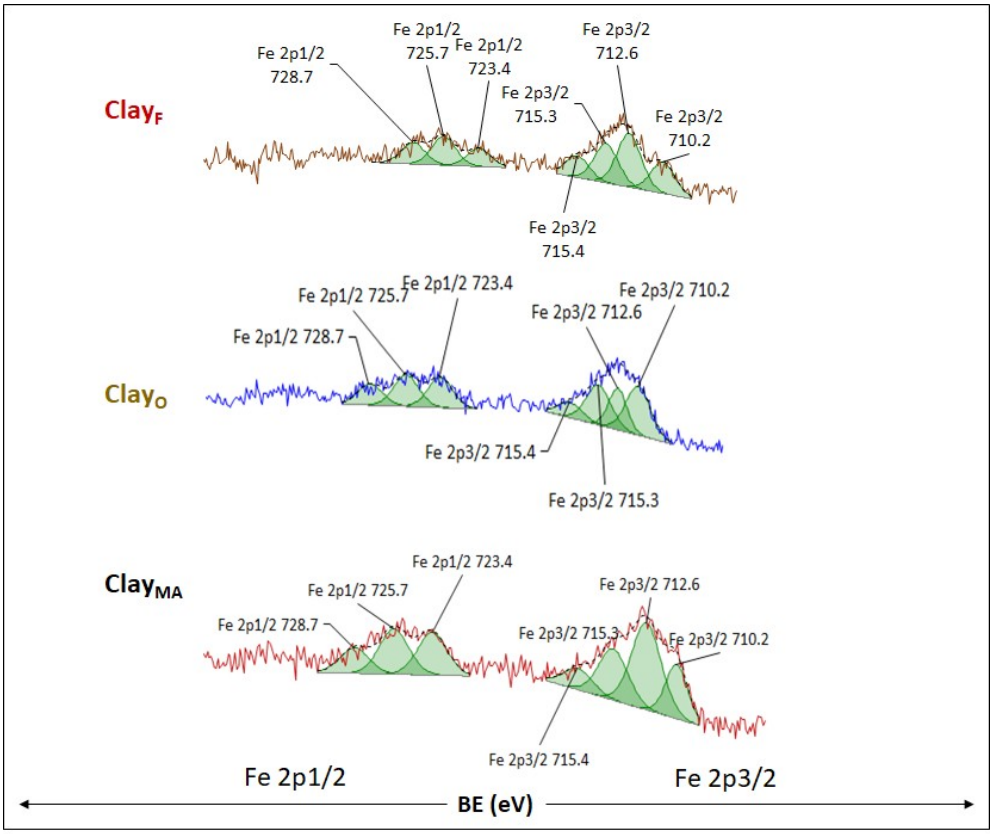

Fig. 3. High XPS spectra of Fe 2p of all pristine clays.

For all the samples, the Fe $2p_{1/2}$ peak appears to be composed by three components at 728.7, 725.7, and 723.4 eV for all the samples, whereas the Fe $2p_{3/2}$ peak results from the overlapping of four contributions at BE values of 710.2, 712.6, 715.3 and 715.4 eV. These values of BE are related to the presence of Fe^{3+} and Fe^{2+} in the form of oxides in the clay minerals (Elmi et al., 2016; Handbook of X-ray Photoelectron Spectroscopy, 1992; Naumkin et al., 2012).

The other elements as C 1s, O 1s, Al 2s, and Si 2p show a single peak attributed to them. In addition, the peak Al 2p were identified at 74.14, 73.25 and 74.91 eV for $Clay_O$, $Clay_F$ and $Clay_{MA}$, respectively. The peak at 285.06 or 285.13 eV attributed to C 1s is a result of surface-atmosphere interactions or residual precursors (Ihekweme et al., 2020; Todea et al., 2013), whereas the peak at closer to 532 eV for oxygen is due to the

elemental oxygen, oxides, oxygen in water and metal oxides associated with the elements (Ihekweme et al., 2020). Al 2s at 119.5 eV and Si 2p at 103 eV are attributed to the chemical bonds as Si-O-Si, Si-O-Al or both atoms coordinated with other elements, typical of these type of materials (Elmi et al., 2016; Tissot et al., 2016). These element peaks were deconvoluted in three components as shown in their high XPS spectra (Fig. 4).

For Si 2p, the presence of the three components in all clays suggest that the Si atoms are tetrahedral coordinated with oxygen by Si-O-Si and Si-O-Al, which confirm the presence of the bonds in these materials (Elmi et al., 2016). The presence of three components for Al 2s and the peak Al 2p close to 74 eV suggest the existence of the same coordination as Si and the presence of Al-OH bonds in tetrahedral or octahedral coordination. From literature, the binding energy values of Al 2p from both tetrahedral and octahedral Al atoms are intermediate between the octahedral and tetrahedral binding energy values (Elmi et al., 2016). Since our BE values at 74.14, 73.25 and 74.91 eV for $Clay_O$, $Clay_F$ and $Clay_{MA}$, respectively, suggest that the Al atoms at the surface in the clays have tetrahedral or/and octahedral coordination.

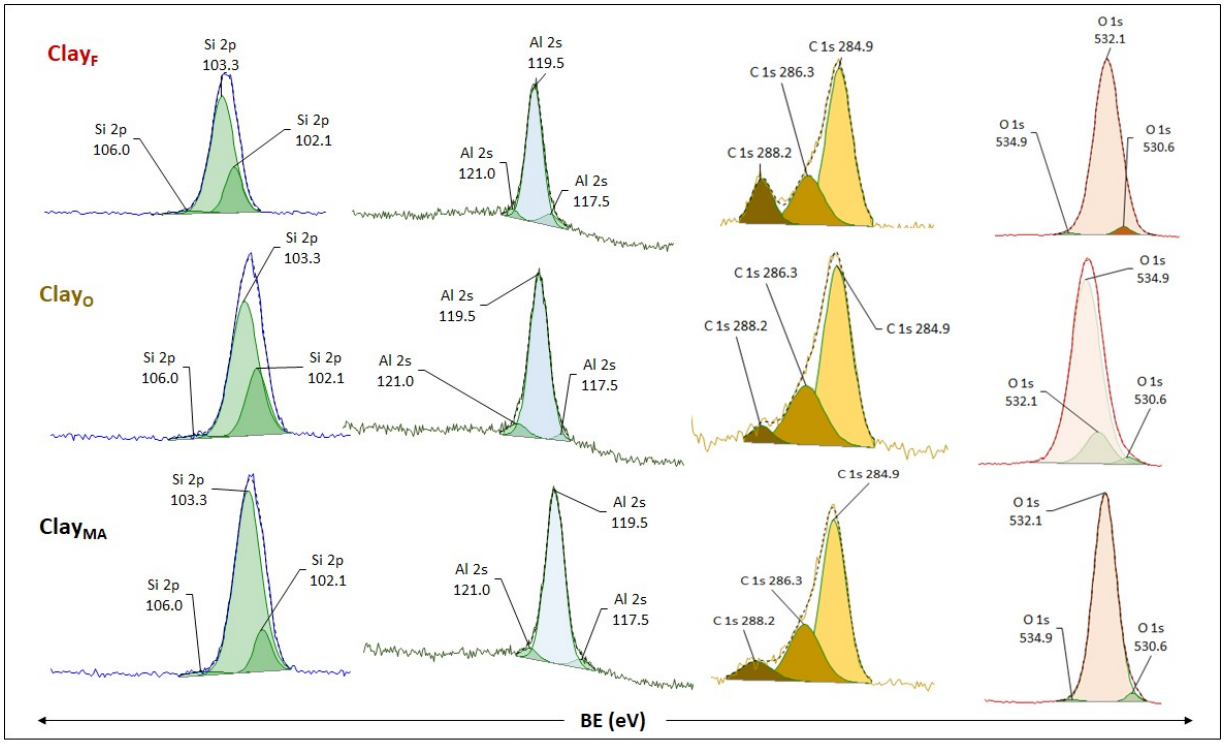

340

341 **Fig. 4.** High XPS spectra of Si 2p, Al 2s, C 1s and O 1s of all pristine clays.

342

343 Samples obtained by modifying Clay$_{MA}$ with Cu or Zn were also analyzed by XPS.
344 Concerning the major components, their XPS profiles were similar to that of the pristine
345 clay. The BE regions of Cu 2p and Zn 2p were also investigated to have information
346 about the nature and the surface concentration of the metals. Peaks of Cu $2p_{1/2}$ and Cu
347 $2p_{3/2}$ were detected at 953.48 eV and 931.98 eV, respectively, from which a Cu surface
348 amount of 0.47 wt% was calculated. Likewise, in the XPS spectrum of Zn-Clay$_{MA}$, two
349 peaks ascribable to Zn $2p_{1/2}$ and Zn $2p_{3/2}$, respectively, were identified at 1041.11 eV
350 and 1025.21 eV, which allowed of determining a Zn surface content of 0.34 wt%.
351 Noteworthy, both the Cu and Zn concentrations on the surface are similar to those
352 determined by ICP-OES analysis for the bulk (Table 2), which suggests a homogeneous
353 distribution of the metals throughout the Clay$_{MA}$ particles.
354 The XRD pattern of the rawclay from Fez (Fig. 5) is presented to exemplify the
355 identification of the detrital and clay minerals present in these materials. In this sample

(Clay$_F$) there are also non-clay minerals, typically detrital minerals like quartz, mica, and plagioclase, observed in the bulk sample (< 2 mm). Nevertheless, calcite is the most abundant non clay mineral that occurs even in the clay size fraction (reflection at 3.86 Å, 3.04 Å, and 2.50 Å). Illite is indicated by the values for d_{001} of 10.1 Å and d_{002} of 5.02 Å, which are not influenced by EG-solvated conditions. Kaolin mineral, probably kaolinite, was identified by their d_{001} and d_{002} reflections at 7.06 Å and 3.59 Å. There is also chlorite detected by 00l reflections as recommended by Moore and Reynolds (1997), with reflections around 7 Å, 4.74 Å, and 3.55 Å. Regarding smectite, it was identified combining the patterns of air-dry samples with glycolated and heated profiles. Thus, the broad reflection in the region of low-2θ side, at 15.87 Å in the air-dry sample was expanded to approximately 17 Å in the EG-solvated. After heating, this peak collapses to 10 Å, which is characteristic of this mineral phase. The iron oxyhydroxide goethite is present, but in trace amounts, as indicated by weak, but typical reflection at 2.69-2.70 Å. In this sample, the higher adsorption potential should be given by the smectite (Bencheqroun et al., 2019b). The Clay$_O$ has also illite and kaolin mineral as common with Clay$_F$, but the other phases are interstratified vermiculite-chlorite, and goethite. In this case, the suitability for adsorption is conferred mainly by the interstratified clay minerals vermiculite-chlorite and illite-vermiculite. The adsorption potential could be somehow increased also by the iron oxyhydroxide goethite.

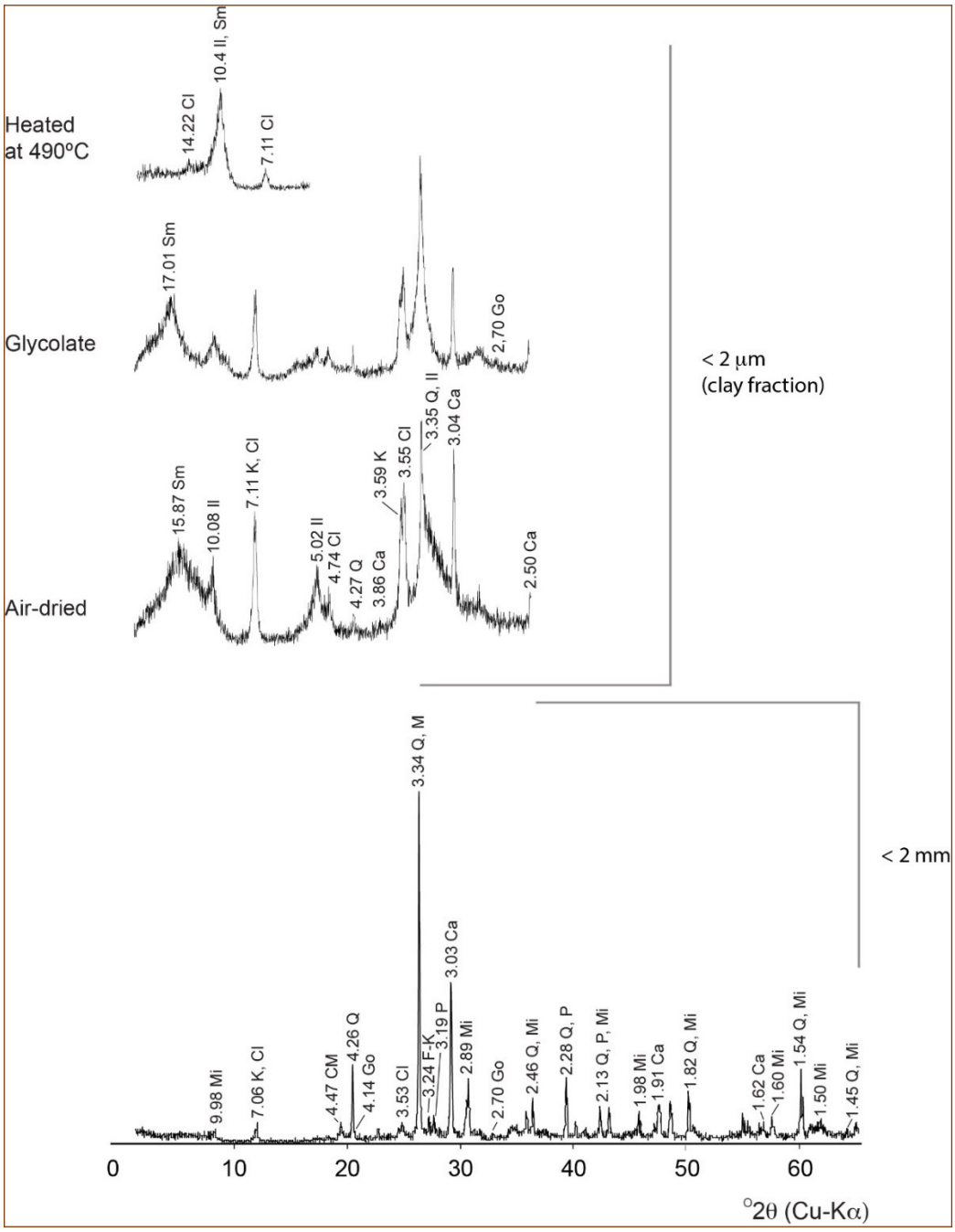

375

376 **Fig. 5.** XRD patterns of clay material – $Clay_F$, showing the analysis of two size fractions
377 (2 mm and < 2 μm), with the respective treatments that allow identification of clay
378 minerals. Q – Quartz; Mi – Mica; P – Plagioclase; F-K – K-Feldspar; Ca – Calcite; CM
379 – Clay Minerals; Il – Illite; C – Chlorite; K – Kaolinite; Sm – Smectite; Go – goethite.

380

381 **3.2 Fenton-type reaction of the dyes**

The choice of the oxidation reaction is reliant on the nature of the pollutants and their stability in Fenton-type reaction. Concerning the pollutants, they were chosen due their presence in aqueous effluents in Morocco. Congo Red (CR) and Tartrazine (Tar) are azo molecules, di and mono, respectively, while caffeine (Caf) is a purine molecule based in a xanthine core with two fused rings, a pyrimidinedione and imidazole (Fig. 6).

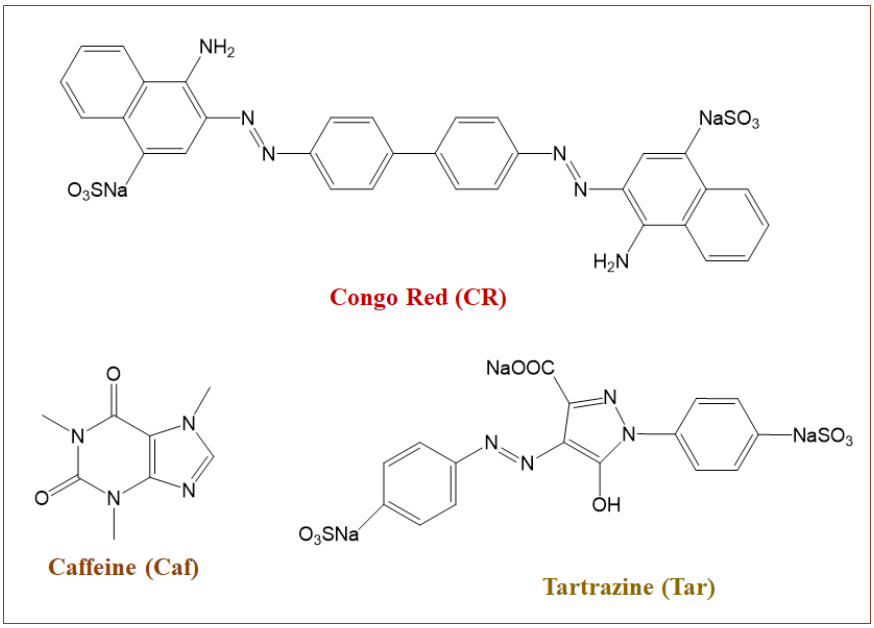

Fig. 6. Chemical structure of the dyes.

Tar and Caf were studied by a typical Fenton-type reaction with all the pristine clays. Moreover, in order to improve the efficacy of the degradation of these pollutants, two new heterogeneous catalysts were prepared with $Clay_{MA}$ by the introduction of copper ($Cu\text{-}Clay_{MA}$) or zinc ($Zn\text{-}Clay_{MA}$).

The catalytic results obtained with the different heterogeneous catalysts for the degradation of Tar and Caf through Fenton-type reaction, using the experimental conditions determined in (Assila et al., 2023), are display in Fig. 7 and 8. Blank runs were also made in the presence of only hydrogen peroxide or raw clays. Hydrogen peroxide by itself was unable to degrade the dyes; indeed, only 4 % of conversion was

399 determined after 5 h of reaction. Similarly, the adsorption tests showed that the clays
400 were able to remove less than 3 % of the dyes after 5 h of reaction. These results suggest
401 that the simultaneous presence of H_2O_2 and clays is required to successfully remove
402 dyes from aqueous media through the Fenton-type reaction.
403 Fig. 7 displays the results for Tar and Caf degradation in terms of both pollutant's
404 conversion and TOC, after 5 h of reaction in the presence of the clay catalysts.

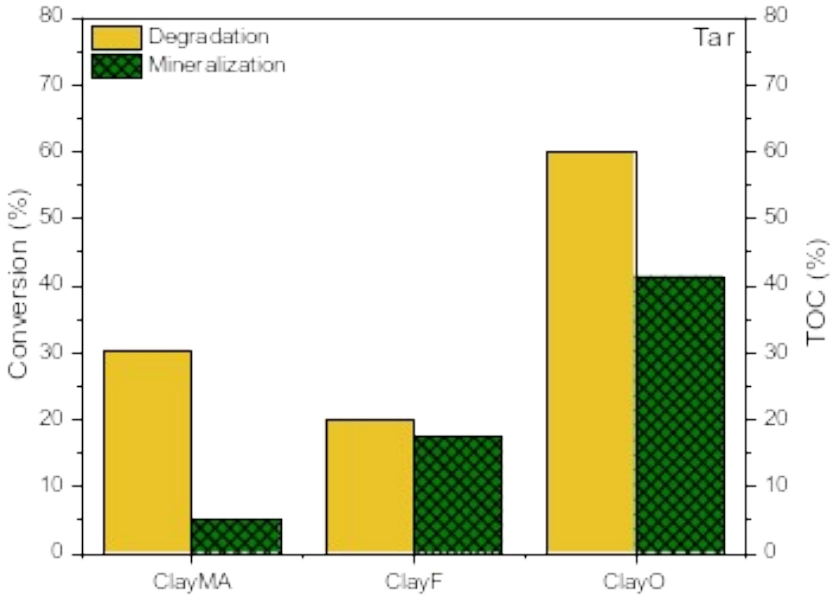

405

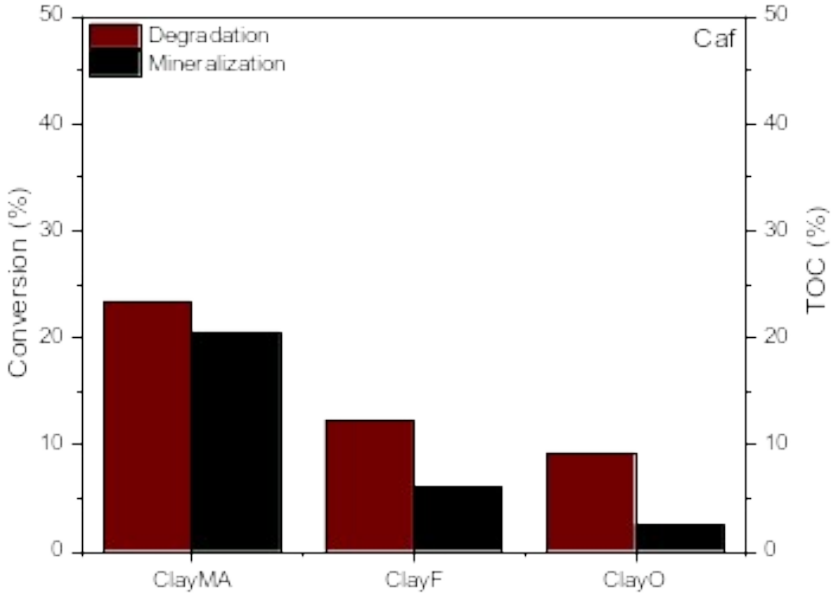

406
407 **Fig. 7**. Conversion and TOC percentages after Tar and Caf degradation by Fenton-type
408 reaction in presence of $Clay_{MA}$, $Clay_F$, and $Clay_O$. Reaction conditions: 250 mL of dye
409 solution (30 ppm); 5 mL of H_2O_2 solution (90 mM); T = 40 ºC; pH = 3.0; 0.2 g of
410 catalyst.

411 All clays are more effective in degrading Tar than Caf, with $Clay_O$ showing the best
412 performance, achieving in the case of Tar 60 % of conversion and 41.5 % of
413 mineralization. This suggests that the catalyst can favor the formation of hydroxyl
414 ($HO^{\bullet}$) radicals responsible for Tar degradation. On the other hand, $Clay_{MA}$ and $CLay_F$
415 show a much lower removal capacity, reaching conversion values of 30.5 and 20.1 %,
416 respectively. Notably, although the conversion is higher for ClayMA, the degree of
417 mineralization for this catalyst is only 5 %.
418 In the case of Caf degradation, the behavior of the clay catalysts are different with
419 $Clay_{MA}$ the best one, with 23.4 % in conversion. The low values obtained for the Caf
420 conversion in the presence of the raw clays confirm that the caffeine molecule is very
421 stable and these catalysts do not reach to convert all 30 ppm, despite the better

mineralization degree for $Clay_{MA}$ (20.5 %), follow by $Clay_F$ with 6 % and 2.5 % for $Clay_O$. These catalytic results are not only dependent of the molecular structure of the pollutants but also to the chemical composition and the geological place of the clays. For Tar degradation, a clay rich in iron at surface (5.98 wt%) enhances the Fenton-type reaction ($Clay_O$), follow by $Clay_F$ which has homogeneous distribution of the iron with higher amount of calcium (Tables 2 and 3).

To investigate the effect of Zn or Cu addition on the catalytic behavior of $Clay_{MA}$, the Fenton-like reaction was studied using both Zn-$Clay_{MA}$ and Cu-$Clay_{MA}$ as heterogeneous catalysts for the removal of both dyes. The choice of these metals was related to their performance in Fenton-type reactions when added to different inorganic materials for preparing bimetallic catalysts [6, 31-33]. The pertinent results are compared with those obtained for the pristine clay in Fig. 8.

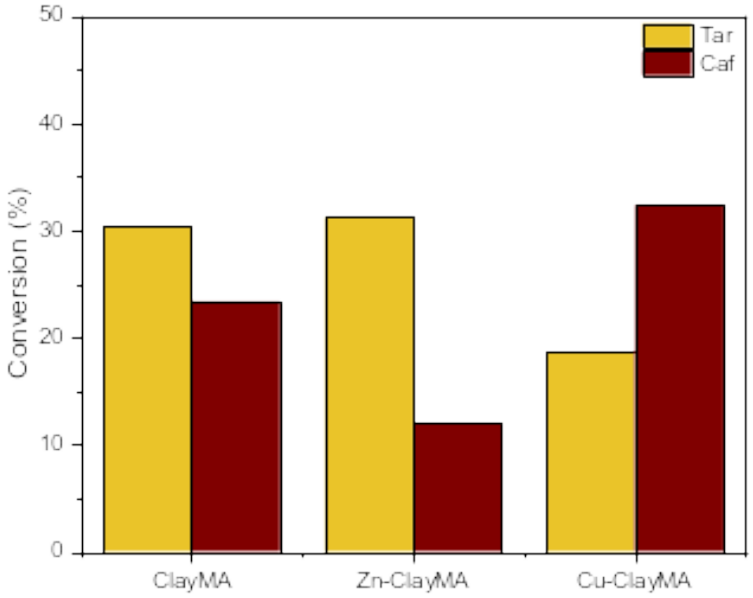

Fig. 8. Conversion of Tar and Caf by Fenton-type reaction in the presence of $Clay_{MA}$, Zn-$Clay_{MA}$, and Cu-$Clay_{MA}$. Reaction conditions: 250 mL of dye solution (30 ppm); 5 mL of H_2O_2 solution (90 mM); T = 40 ºC; pH = 3.0; 0.2 g of catalyst.

438

439 Zn-$Clay_{MA}$ and $Clay_{MA}$ are the same behavior for the Tar conversion, which suggest that
440 the presence of Zn do not improve the degradation of tratrazine. In addition, the
441 presence of copper is worst. The choice of these metals are associated to their
442 performance as bimetallic catalysts in different inorganic materials in Fenton-type
443 reactions [(Assila et al., 2023; Fu et al., 2022; Santos et al., 2021; Usman et al., 2023).
444 On the other hand, for Caf degradation the presence of copper improve the oxidation of
445 the molecule (32.4 %) compared to the pristine clay. The presence of Zn is very harmful
446 for the catalyst, since the catalyst lost their activity in the degradation of caffeine.
447 Taking in account all the catalytic results obtained with Fenton-type reaction, the best
448 catalyst was the raw clay from Ourika region ($Clay_O$) for Tar degradation and Cu-
449 $Clay_{MA}$ for Caf oxidation.
450 Being not stable in the acidic medium used in the Fenton-type reaction because of its
451 precipitation, the Congo red (CR) dye degradation was instead performed through the
452 electro Fenton-type reaction, using $Clay_F$ and $Clay_O$ modified electrodes. In our previous
453 work, CR was degraded using Fe-zeolite modified catalysts based on different zeolite
454 structures (Bencheqroun et al., 2022c). In that case, the Fe-(H)ZSM-5 modified
455 catalysts showed the best degradation results due to the acidic properties of the MFI
456 structure (Bencheqroun et al., 2022c).

457 The cycle voltammmetry studies between -2.0 V and +2.0 V *vs.* SCE potential with the
458 clay-modified electrodes based on $Clay_O$ and $Clay_F$ on Carbon Toray (CT) were
459 performed with a scan rate of 50 mVs^{-1} in the presence of NaCl as electrolyte or with
460 the CR dye (25 ppm), at room temperature (Fig. 9).

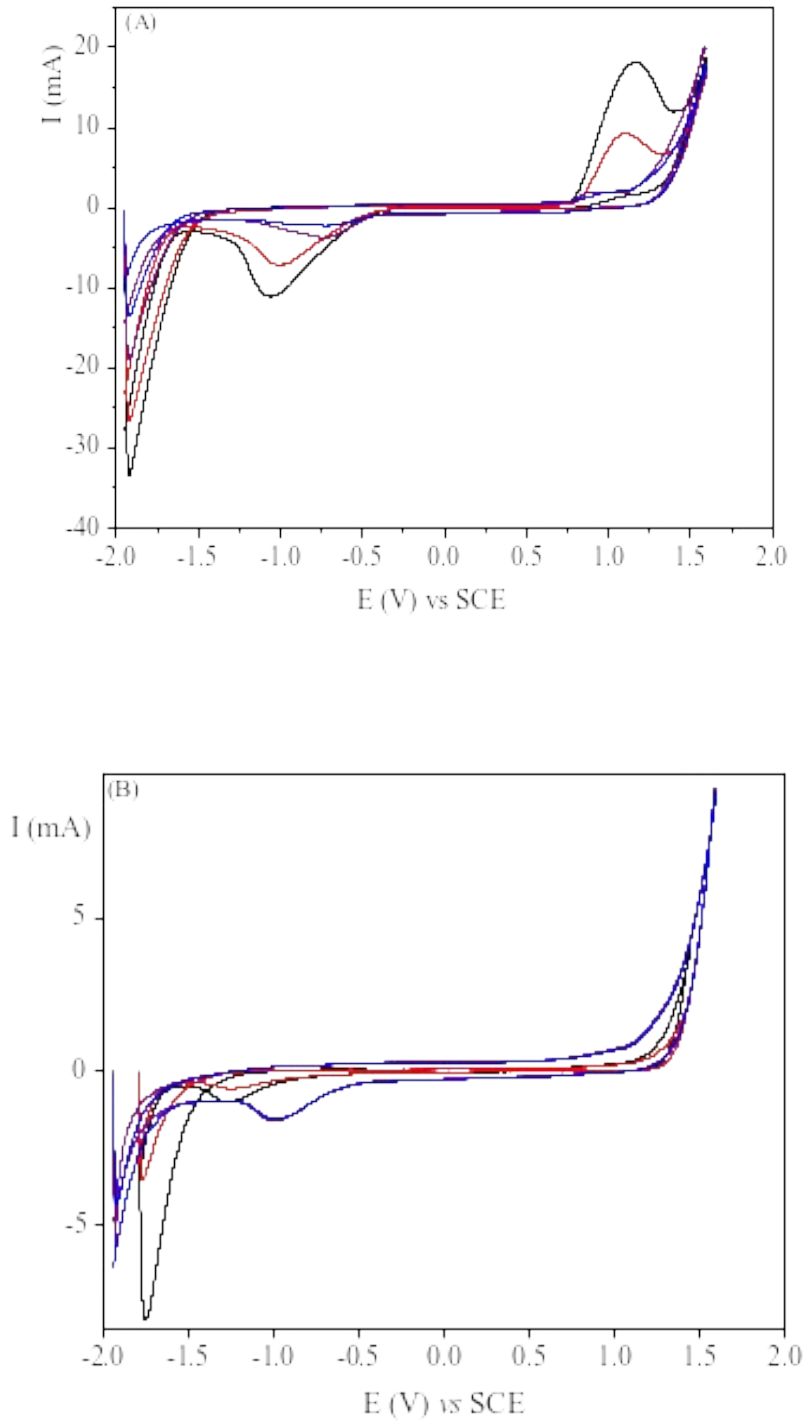

461 **Fig. 9.** Cyclic voltammograms of the CME based on: A) $Clay_F$ and B) $Clay_O$ at a scan
462 rate of 50 mVs^{-1}, in the absence of dye (black and red curves) and in the presence of 25
463 ppm of CR (blue and violet curves) in NaCl (0.10 M).
464

The electro behavior of both the CME are different and it is probably related to the presence of different iron species, *i.e.* the Fe(II)/Fe(III) couple, or other cations present in on the surface of both clays, as determined by XPS and ICP-OES analysis (Tables 2 and 3). The $Clay_O$-modified electrode in absence of CR dye (black and red curves) show one irreversible cathodic process at -1.3 V *vs.* SCE in 0.1 M NaCl medium. For the raw clay from Fez City, an anodic redox process is observed at 1.2 V *vs.* SCE, and in the reverse scan of the potential, a reduction peak can be seen at -1.0 V *vs.* SCE.

In the presence of CR dye (blue and violet curves), both CME are active and show an increment of the anodic process, attributed to the catalytic activity of the catalysts. The oxidation of CR starts at 0.8 V and 1.1 V *vs.* SCE for $Clay_F$ and $Clay_O$, respectively, after the oxidation of Fe(II) into Fe(III), indicating that the presence of Fe(III) species on the electrode surface is necessary for the oxidation of this organic dye (Bencheqroun et al., 2022c).

The rate-determining step of the CR oxidation process can be determined by voltammetry studies where the slope of the logI (mA) *vs*. v (mVs^{-1}) curves in 0.1 M NaCl medium corresponds to 0.62 and 0.55 to $Clay_F$ and $Clay_O$, respectively and these values are consistent with a kinetic of the electrochemical reaction governed by the diffusion step (Bencheqroun et al., 2022c).

The electrolysis of CR (50 ppm, 0.072 mM) with the CME was performed with an applied potential of 2.0 V *vs.* SCE, at room temperature, without hydrogen peroxide. Both clays as CME are efficient in degrading the dye by electro Fenton-type reaction, but $Clay_F$ is more effective since its remove the dye in less time of reaction than $Clay_O$. Fig. 10 shows the results obtained for $Clay_F$-modified electrode in the beginning and after 2 h of reaction, as well as the evolution of the CR conversion over the modified clay electrode.

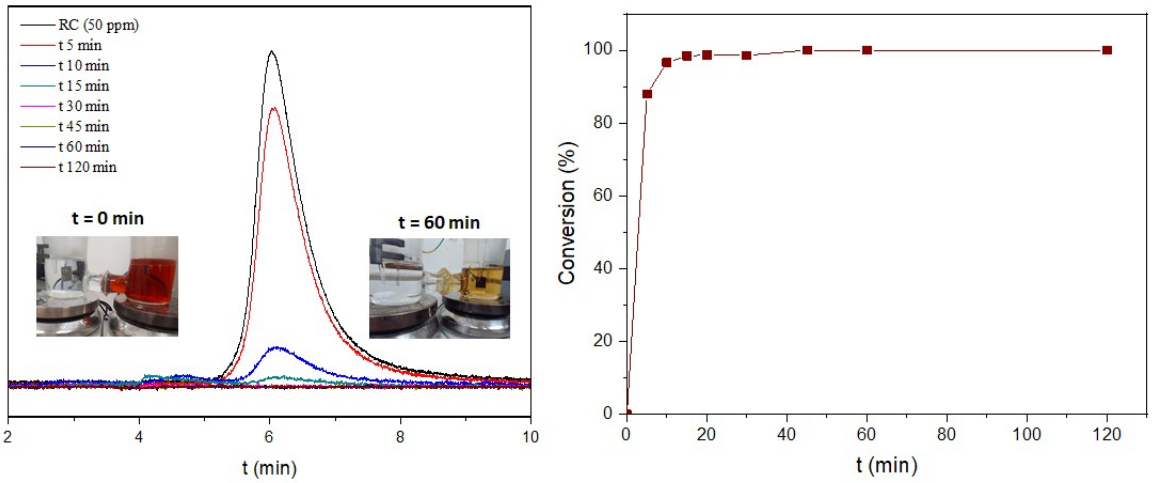

Fig. 10. HPLC-UV/vis chromatograms and the conversion of CR (■) *vs.* electrolysis time for the electroxidation of CR in the presence of $Clay_F$-modified electrode.

The results show that degradation occurs very fast since 81 % of the CR molecule is degraded after 5 min, being fully oxidized after 45 min of reaction (Fig. 10). At the end of reaction (2 h), TOC was determined and 67 % of mineralization was calculated. A similar value of mineralization (64 %) was previously obtained with the best Fe(H)ZSM5-modified electrode (Bencheqroun et al., 2022c). However, on the $Clay_F$-modified electrode degradation of the dye appears to be faster than on the electrodes modified with Fe-MFI zeolites, on which only 74 % of CR conversion was achieved after 10 min of reaction (Bencheqroun et al., 2022c).

Fig. 11 shows the cyclic voltammograms recorded before and after the electrolysis in the presence of CME modified with $Clay_F$.

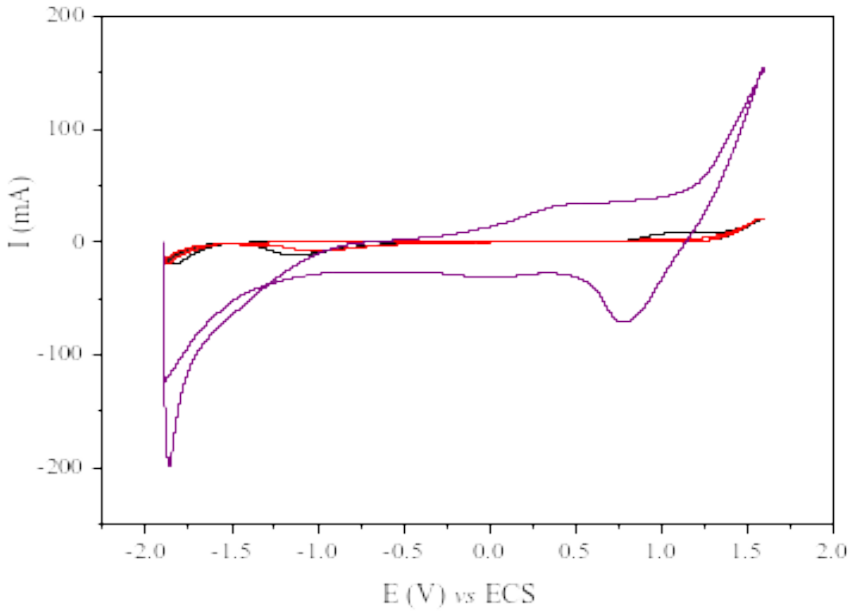

Fig. 11. Cyclic voltammograms of CME based on ClayF, recorded at 50 mVs^{-1} before (red and black curves) and after the electrolysis (violet curve) of Congo Red dye (0.072 mM) in NaCl (0.10 $molL^{-1}$).

After electrolysis, an increase in the overall current intensities was observed, which is attributed to the restructuring of the electrode surface, including an increase in the active surface, due to the oxidative treatment during electrolysis. This increase may also be due to the contribution of current intensities resulting from the oxidation of some electrolysis products. The same behavior was observed after the electrolysis of CR with zeolite modified catalysts (Bencheqroun et al., 2022c).

HPLC-UV/vis and IC (ionic chromatographic) analyses were employed to quantify the products at the end of reaction. The results reveal the presence of sulfate ions and several low molecular weight carboxylic acids, which are the byproducts of the CR rings opening triggered by the hydroxyl radicals produced during the electro-Fenton reaction (Fig. 12 and Table 4).

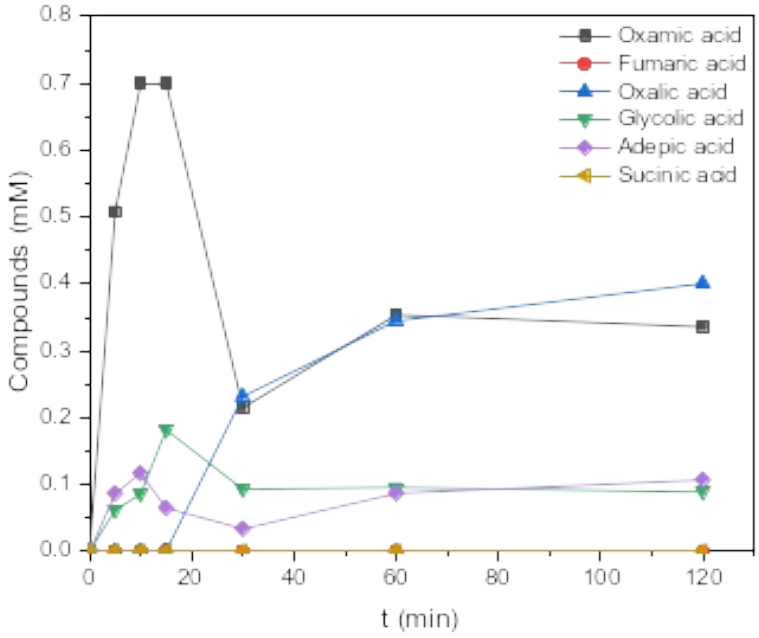

520

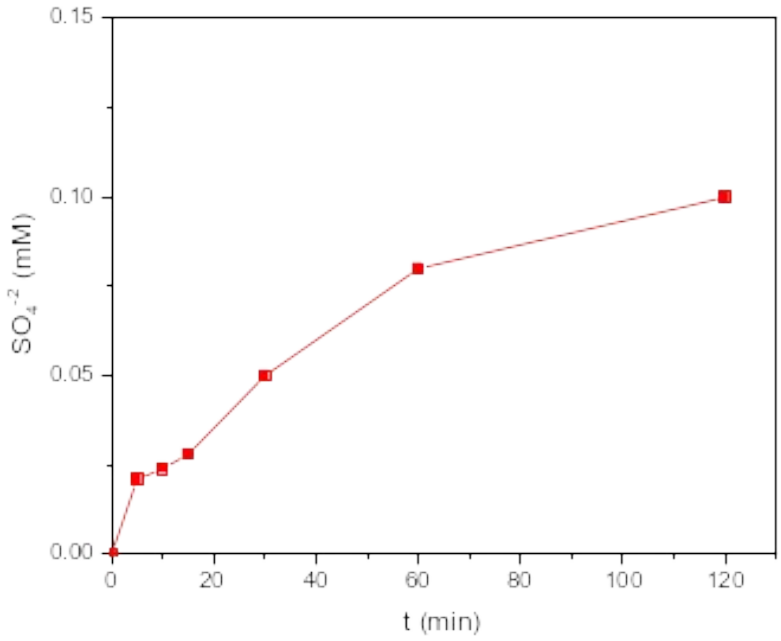

521

522 **Fig. 12.** The evolution of the compounds and sulfate ions during the electrolysis of CR

523 in presence of CME based in $Clay_F$.

524

525

Table 4. Identification of the byproducts

Byproduct		Concentration (mM)	Percentage (%)
Oxamic acid	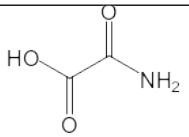	0.336	36
Oxalic acid	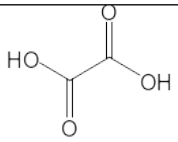	0.401	43
Glycolic acid	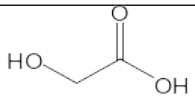	0.089	9.5
Fumaric acid	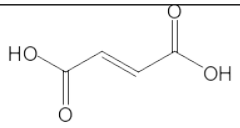	0.011	<0.1
Succinic acid	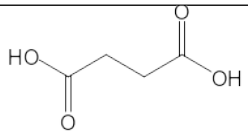	$0.5x10^{-5}$	<0.01
Adepic acid	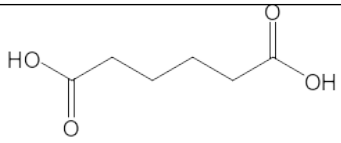	0.117	11.5

The major compounds identified at the end of electrolysis were oxamic, oxalic and adipic acids, and sulfate ions. These recalcitrant products result from the degradation of the dye by the electro-generation of the oxygenated radical species and the presence of Fe(III)-hydroperoxo species. These species come from the oxidation of water in the adopted oxidative conditions since the presence of oxygen is produced at 2.0 V *vs.* SCE (Bencheqroun et al., 2022c). The higher mineralization rate (67 %) determined for $Clay_F$ as CME probably is related to the chemical composition of this raw clay as well as the geological place. As mentioned before, this clay is rich in calcium and has a homogeneous distribution of iron, which enhance the electro-Fenton reaction.

4. Conclusion

In this study, the Fenton-type reaction was used as the oxidative process for degrading two organic pollutants (Tar and Caf), using three raw clays from Morocco as heterogeneous catalysts. Under the adopted experimental conditions, these clays are more effective in oxidizing tartrazine than caffeine. The best catalytic results were obtained in the presence of $Clay_O$ and $Clay_{MA}$ with 60.0 and 23.4 % conversion, and 41.0 and 20.5 % mineralization for Tar and Caf, respectively. The introduction of zinc or copper into $Clay_{MA}$ does not lead to a significant improvement in the degradation of Tar, the conversion of the metal-containing clay being equal to that of the starting one. However, Cu-$Clay_{MA}$ enhances the oxidation of the caffeine molecule (32.4 %) compared to the pristine clay. Moreover, the electro-Fenton-type reaction was found to promote the oxidation of CR at room temperature with a high mineralization degree (67 %), avoiding the use of redox agents. Our study shows that the raw clays from Morocco can be successfully applied in water treatments as a low-cost heterogeneous catalyst for a sustainable process.

Conflicts of interest

There are no conflicts of interest to declare.

Acknowledgments

O.A. and Z.B. thank to ERASMUS+ Program for the mobility PhD grants. This research work has been funded by national funds funded through FCT/MCTES (PIDDAC), (Fundação para Ciência e Tecnologia, FCT) over the projects: LA/P/0045/2020 (ALiCE), UIDB/50020/2020 and UIDP/50020/2020 (LSRE-LCM),

Centre of Chemistry (UID/QUI/0686/2020) and project BioTecNorte (operation NORTE-01-0145-FEDER-000004), supported by the Northern Portugal Regional Operational Programme (NORTE 2020), under the Portugal 2020 Partnership Agreement, through the European Regional Development Fund (ERDF).

References

Anastas P.T., Zimmerman J.B., The Molecular Basis of Sustainability, Chem., 20161, 10–12, http://dx.doi.org/10.1016/j.chempr.2016.06.016

Assila, O., Barros, Ó., Fonseca, A.M., Parpot, P., Soares, O.S.G.P., Pereira, M.F.R., Zerrouq, F., Kherbeche, A., Rombi, E., Tavares, T., Neves, I.C. Degradation of pollutants in water by Fenton-like oxidation over LaFe-catalysts: Optimization by experimental design, Microporous and Mesoporous Materials, 2023, 3491, 112422, DOI:10.1016/j.micromeso.2022.112422.

Axon S., James D., The UN Sustainable Development Goals: How can sustainable chemistry contribute? A view from the chemical industry, Curr. Opin. Green Sustain. Chem. 2018, 13, 140–145. https://doi.org/10.1016/j.cogsc.2018.04.010.

Bencheqroun, Z., Mrabet, I.El, Kachabi, M., Nawdali, M., Valdés, H., Neves, I., Zaitan, H., Removal of basic and acid dyes from aqueous solutions using cone powder from Moroccan cypress Cupressus sempervirens as a natural adsorbent, Desalination and Water Treatment, 2019a, 166, 387–398., https://doi.org/10.5004/dwt.2019.24514

Bencheqroun, Z., Mrabet, I.El, Kachabi, M., Nawdali, M., Neves, I., Zaitan, H. Removal of Basic Dyes from Aqueous Solutions by Adsorption onto Moroccan Clay (Fez City), Mediterranean Journal of Chemistry 2019b, 8(2), 158-167

Bencheqroun, Z., Sahin, N.E., Soares, O.S.G.P., Pereira, M.F.R., Zaitan, H., Nawdali, M., Rombi, E., Fonseca, A.M., Parpot, P., Neves, I.C. Fe(III)-exchanged zeolites as efficient electrocatalysts for Fenton-like oxidation of dyes in aqueous phase, Journal of Environmental Chemical Engineering 2022b, 10, 107891. https://doi.org/10.1016/j.jece.2022.107891.

590 Bergaya, F. The meaning of surface area and porosity measurements of clays and
591 pillared clays, J. Porous Mater. 1995, 2, 91–96.

592 Brillas, E., Sires, I., Oturan, M.A. Electro-Fenton process and related electrochemical
593 technologies based on Fenton's reaction chemistry. Chem. Rev. 2009, 109, 6570-
594 6631.

595 Chaplin, B.P., 2014. Critical review of electrochemical advanced oxidation processes
596 for water treatment applications. Environ. Sci. Process. Impacts 16, 1182-1203.

597 Elmi, C., Guggenheim, S., Giere, R., Surface crystal chemistry of phyllosilicates using
598 X-ray photoelectron spectroscopy: a review. Clay Clay Miner. 2016, 64 (5), 537–551

599 Ferreira, M., Biernacka, I. K., Fonseca, A.M., Neves, I.C., Soares, O.S.G.P., Pereira,
600 M.F.R., Figueiredo, J.L., Parpot, P. Study of the Electroreactivity of Amoxicillin on
601 Carbon Nanotube-Supported Metal Electrodes, ChemCatChem 2018, 10, 4900–
602 4909.

603 Fida, H.; Zhang, G.; Guo, S.; Naeem, A. Heterogeneous Fenton Degradation of Organic
604 Dyes in Batch and Fixed Bed Using La-Fe Montmorillonite as Catalyst. J. Colloid
605 Interface Sci. 2017, 490, 859–868, doi:10.1016/j.jcis.2016.11.085.

606 Fu, W., Yi, J., Cheng, M., Liu, Y., Zhang, G., Li, L., Du, L., Li, B., Wang, G., Yang, X.,
607 When bimetallic oxides and their complexes meet Fenton-like process, J. Hazard.
608 Mater., 424 (2022) 127419, doi.org/10.1016/j.jhazmat.2021.127419;

609 Fu, W., Yi, J., Cheng, M., Liu, Y., Zhang, G., Li, L., Du, L., Li, B., Wang, G., Yang, X.
610 When bimetallic oxides and their complexes meet Fenton-like process, Journal of
611 Hazardous Materials, 2022, 424, 127419,
612 https://doi.org/10.1016/j.jhazmat.2021.127419.

613 Garrido-Ramírez, E.G., Mora, M.L., Marco, J.F., Ureta-Zanartu, M.S., Characterization
614 of nanostructured allophane clays and their use as support of iron species in a
615 heterogeneous electro-Fenton system. Appl. Clay Sci. 2013, 86, 153-161.

616 Handbook of X-ray Photoelectron Spectroscopy: A Reference Book of Standard Spectra
617 for Identification and Interpretation of XPS Data, ed. Jill Chastain, Physical
618 Electronics Division, Perkin-Elmer Corporation, 1992.

619 Herney-Ramirez, J., Vicente, M.A., Madeira, L.M., Heterogeneous photo-Fenton
620 oxidation with pillared clay-based catalysts for wastewater treatment: a review. Appl.
621 Catal. B Environ. 2010, 98, 10-26.

622 Ihekweme, G.O., Shondo, J.N., Orisekeh, K.I., Kalu-Uka, G.M., Nwuzor, I.C.,
623 Onwualu, A.P. Characterization of certain Nigerian clay minerals for water
624 purification and other industrial applications, Heliyon 2020, 6, 03783.

625 Jiang, J.Q., Ashekuzzaman, S.M., Hargreaves, J.S.J., Mcfarlane, A.R., Badruzzaman,
626 A.B.M., Tarek, M.H. Removal of arsenic (III) from groundwater applying a reusable
627 Mg-Fe-Cl layered double hydroxide, J. Chem. Technol. Biotechnol. 90 (2015) 1160–
628 1166; *Mediterranean Journal of Chemistry* **2019**, 8(2), 158-167.

629 Kloprogge, J.T. Synthesis of smectites and porous pillared clay catalysts: a review, J.
630 Porous Mater. 1998, 5, 5–41.

631 Liu, Y., Zhao, Y., Wang, J., Fenton/Fenton-like processes with in-situ production of
632 hydrogen peroxide/hydroxyl radical for degradation of emerging contaminants:
633 Advances and prospects, J. Hazard. Mater., 2021, 404, 124191,
634 doi.org/10.1016/j.jhazmat.2020.124191;

635 Ma, H., Zhuo, Q., Wang, B. Electro-catalytic degradation of methylene blue wastewater
636 assisted by Fe2O3-modified kaolin. Chem. Eng. J., 2009, 155, 248e253

637 Naumkin, A.V., Kraut-Vass, A., Gaarenstroom, S.W., Powell, C.J. NIST X-ray
638 Photoelectron Spectroscopy Database, NIST Standard Reference Database 20,
639 Version 4.1, Last Update to Data Content: 2012, http://dx.doi.org/10.18434/T4T88K;

640 Ozcan, A., Ozcan, A.A., Demirci, Y., Sener, E. Preparation of Fe_2O_3 modified kaolin
641 and application in heterogeneous electro-catalytic oxidation of enoxacin., Appl.
642 Catal. B Environ. 2017, 200, 361-371

643 Poza-Nogueiras, V., Rosales, E., Pazos, M., Sanrom, M.A. Current advances and trends
644 in electro-Fenton process using heterogeneous catalysts e A review, Chemosphere,
645 2018, 201, 399-416.

646 Santos, B.L.C., Parpot, P., Soares, O.S.G.P., Pereira, M.F.R., Rombi, E., Fonseca, A.M.,
647 Neves, I.C. Fenton-Type Bimetallic Catalysts for Degradation of Dyes in Aqueous
648 Solutions, Catalysts 2021, 11, 32. https://doi.org/10.3390/ catal11010032

649 Schoonheydt R.A., Clays: from two to three dimensions, in Introduction to zeolite
650 science and practice, H. van Bekkum, E.M. Flanigen, J.C. Jansen (Eds.), Studies in
651 Surface Science and Catalysis, Elsevier, Netherlands, V. 58, 1991, pp 201-239.

652 Tissot, H., Li, L., Shaikhutdinov, S., Freund, H.J. Preparation and structure of Fe
653 containing aluminosilicate thin films. Phys. Chem. Chem. Phys. 2016, 18 (36),
654 25027–25035;

655 Todea, M., Vanea, E., Bran, S., Berce, P., Simon, S., XPS analysis of aluminosilicate
656 microspheres bioactivity tested in vitro. Appl. Surf. Sci. 2013, 270, 777–783.

657 United Nations, 2023,
658 https://www.un.org/sustainabledevelopment/wp-content/uploads/2019/07/UN-SG-
659 Roadmap-Financing-the-SDGs-July-2019.pdf

660 United Nations, Sustainable development knowledge platform, sustainable development
661 goals, 2016. https://sustainabledevelopment.un.org/sdgs

662 Usman, M., Monfort, O., Gowrisankaran, S., Hameed, B.H., Hanna, K., Al-Abri, M.
663 Dual functional materials capable of integrating adsorption and Fenton-based
664 oxidation processes for highly efficient removal of pharmaceutical contaminants,
665 Journal of Water Process Engineering, 2023, 52, 103566.
666 https://doi.org/10.1016/j.jwpe.2023.103566.

667 Wang, J.; Tang, J. Fe-based Fenton-like catalysts for water treatment: Preparation,
668 characterization and modification, Chemosphere, 2021, 276, 130177,
669 doi.org/10.1016/j.chemosphere.2021.130177.

670 Weidler, P.G. BET sample pretreatment of synthetic ferrihydrite and its influence on the
671 determination of surface area and porosity, J. Porous Mater. 1997, 4, 165–169.

672